Available online at www.sciencedirect.com

SciVerse ScienceDirect

Acta Materialia 61 (2013) 6362–6371

Acta MATERIALIA

www.elsevier.com/locate/actamat

Stress dependence of the Peierls barrier of 1/2⟨1 1 1⟩ screw dislocations in bcc metals

R. Gröger [a,*], V. Vitek [b]

[a] Central European Institute of Technology – Institute of Physics of Materials (CEITEC-IPM), Academy of Sciences of the Czech Republic, Žižkova 22, 61662 Brno, Czech Republic

[b] Department of Materials Science and Engineering, University of Pennsylvania, 3231 Walnut Street, Philadelphia, PA 19104, USA

Received 28 May 2013; received in revised form 25 June 2013; accepted 26 June 2013
Available online 12 August 2013

Abstract

The recently formulated constrained nudged elastic band method with atomic relaxations (NEB + r) (Gröger R, Vitek V. Model Simul Mater Sci Eng 2012;20:035019) is used to investigate the dependence of the Peierls barrier of 1/2⟨1 1 1⟩ screw dislocations in body-centered cubic metals on non-glide stresses. These are the shear stresses parallel to the slip direction acting in the planes of the ⟨1 1 1⟩ zone different from the slip plane, and the shear stresses perpendicular to the slip direction. Both these shear stresses modify the structure of the dislocation core and thus alter both the Peierls barrier and the related Peierls stress. Understanding of this effect of loading is crucial for the development of mesoscopic models of thermally activated dislocation motion via formation and propagation of pairs of kinks. The Peierls stresses and related choices of the glide planes determined from the Peierls barriers agree with the results of molecular statics calculations (Gröger R, Bailey AG, Vitek V. Acta Mater 2008;56:5401), which demonstrates that the NEB + r method is a reliable tool for determining the variation in the Peierls barrier with the applied stress. However, such calculations are very time consuming, and it is shown here that an approximate approach of determining the stress dependence of the Peierls barrier (proposed in Gröger R, Vitek V. Acta Mater 2008;56:5426) can be used, combined with test calculations employing the NEB + r method.

Keywords: Screw dislocation; Peierls barrier; Nudged elastic band; Bcc metals; Peierls stress

1. Introduction

The most outstanding aspects of the plastic deformation of single crystals of body-centered cubic (bcc) metals are the rapid increase in the flow stress with decreasing temperature and increasing strain rate, a strong dependence of the flow stress on the orientation of the crystal relative to the loading axes, and the related breakdown of the Schmid law (for reviews, see Refs. [4–8]). It has been firmly established in the last forty years that this plastic behavior results from sessile 1/2⟨1 1 1⟩ screw dislocations whose cores spread into three {1 1 0} planes of the ⟨1 1 1⟩ zone. These dislocations then possess a very high Peierls stress, and their motion does not obey the Schmid law (for reviews, see e.g. Refs. [5,9]). At finite temperatures, their movement is aided by thermal activation via nucleation of pairs of kinks that subsequently migrate easily along the dislocation line [10–13].

While many atomistic calculations of the core structure of 1/2⟨1 1 1⟩ screw dislocations in bcc metals, as well as the stress needed to move them at 0 K (the Peierls stress), have been made (for a recent review, see Ref. [9]), studies of their thermally activated motion are much rarer. In principle, atomistic modeling of the dislocation motion via formation and propagation of kink pairs can be made by molecular dynamics, and several such calculations were performed [14–17]. Notwithstanding, owing to the limited timescale of molecular dynamics studies at room or lower temperatures, such calculations had to be carried out at stresses

* Corresponding author.
E-mail address: groger@ipm.cz (R. Gröger).

1359-6454/$36.00
http://dx.doi.org/10.1016/j.actamat.2013.06.047

and strain rates several orders of magnitude higher than those of interest in the usual deformation experiments. However, such large strain rates may only be encountered in shock loading, but then the deformation process is not controlled by the formation of kink pairs. Instead, other phenomena such as phonon and electron scattering become dominant (see e.g. Refs. [18–21]).

An alternative though more approximate approach is to develop a mesoscopic model based on the reaction rate theory describing the thermally activated process of the formation of pairs of kinks [10–13]. However, when dislocation core effects are involved, such models depend sensitively on the form of the Peierls barrier $V(\xi)$ that the dislocation has to overcome when moving in the crystal along a generally curvilinear coordinate ξ. The reason is that the activation enthalpy, which determines the rate of the dislocation motion, is obtained by integrating over the Peierls barrier, and this integration requires knowledge of the overall shape of this barrier [22–25]. This information is not obtained in the molecular statics calculations, because these reveal only the core structure and the stress at which the dislocation moves at 0 K, i.e., the Peierls stress σ_P. The only information about the Peierls barrier that can be acquired from these calculations is its maximum slope in the direction of the dislocation motion since

$$\sigma_P b = \max(\mathrm{d}V/\mathrm{d}\xi), \tag{1}$$

where V is the energy per unit length of the dislocation, and b is its Burgers vector. At the same time, the dependence of the Peierls stress on the character of the applied load, which is crucial information needed in the analysis of the deformation behavior of bcc metals, is obtained in the molecular statics calculations. This has to be reflected in the corresponding dependence of the Peierls barrier on the type of loading.

In molecular statics calculations that apply a pure shear stress parallel to the Burgers vector of a $1/2\langle 1\,1\,1\rangle$ screw dislocation, the Peierls stress was generally found to depend on the orientation of the maximum resolved shear stress plane (MRSSP) [2,5,26–28]. This dependence is the origin of the so-called twinning–antitwinning asymmetry found in virtually all bcc metals [4]. However, calculations in which the stress tensor corresponds to tension/compression revealed a strong dependence of the Peierls stress on the shear stress applied perpendicular to the Burgers vector [2,26–28]. This stress does not contribute to the Peach–Koehler force on the dislocation, but affects the magnitude of the Peierls stress indirectly by modifying the structure of the dislocation core. Both the effect of the orientation of the MRSSP and the shear stress perpendicular to the Burgers vector imply that the Peierls barrier is not a fixed function determined purely by the material, as often assumed, but is an explicit function of the applied stress tensor. This is one of the major results of molecular statics studies of the structure and motion of $1/2\langle 1\,1\,1\rangle$ screw dislocations in bcc metals published recently [2]. Moreover, this conclusion is most likely general whenever the dislocation core is not planar. For example, an analogous conclusion was reached in the study of the Peierls barrier of the sessile Lommer–Cottrell dislocation [17]. Consequently, knowledge of the dependence of the Peierls barrier on the applied stress tensor is essential for obtaining the appropriate stress dependence of activation enthalpies and thus to develop a mesoscopic model of thermally activated dislocation motion that includes this dependence.

The calculation of the Peierls barrier can be made using the nudged elastic band (NEB) method, originally developed for studies of chemical reactions [29,30]. Within this method, the minimum energy path of the dislocation between two neighboring lattice sites of the same energy is found and the variation in the dislocation energy along this path is identified with the Peierls barrier. Such calculations were made recently using several empirical schemes to describe the interaction between the atoms as well as methods based on the density functional theory (DFT) [1,17,31–34].

The goal of the present study is to investigate the dependence of the Peierls barrier on the applied shear stresses parallel and perpendicular to the slip direction that were found to control the Peierls stress [2,27]. For this purpose the Peierls barrier and its stress dependence were determined using the NEB method with constrained atomic relaxations (NEB + r), which the present authors formulated recently [1]. While the present calculations have been carried out mainly using the bond order potential for tungsten [35], the findings are likely to be more general and apply broadly to all bcc metals.

In these calculations, it is considered that the dislocation may move by elementary steps on three $\{1\,1\,0\}$ planes of the zone of the common $\langle 1\,1\,1\rangle$ slip direction, as revealed by molecular statics calculations of the dislocation motion at 0 K [2,27]. First, the variation in the Peierls barrier is studied when a pure shear stress parallel to the Burgers vector is applied in planes inclined with respect to the $\{1\,1\,0\}$ plane on which the dislocation glide takes place. Next, the Peierls barriers are evaluated for the dislocation motion on the three $\{1\,1\,0\}$ planes of the $[1\,1\,1]$ zone under zero and applied positive and negative shear stresses perpendicular to the slip direction as well as for the combination of shear stresses parallel and perpendicular to the slip direction. The corresponding Peierls stresses determined from the maximum slopes of these barriers are then compared with those found in molecular statics calculations at 0 K. This comparison illustrates the full consistency of the two approaches. In addition, the case of uniaxial loading is also investigated. Finally, the Peierls barriers obtained from the NEB + r calculations are compared with those estimated previously [3] using only knowledge of the Peierls stress, and the limits of the latter approximate but computationally much less demanding approach are assessed.

2. Theoretical and computational background

Within the NEB method [29,30,36,37], the path of a given system is viewed as a chain of states between its

two a priori known configurations. This chain of states is then evolved towards the minimum energy path through the configurational space. Traditionally, the NEB force has been thought of as a vector of $3N$ components, where N is the number of particles in the system. This NEB force is then used to update all degrees of freedom (DOF) associated with these particles, while calculating the energy of the system using suitable interatomic potentials or first-principles methods. It was shown recently [1] that, while this approach provides the correct amplitude of the Peierls barrier, its shape is not predicted with acceptable accuracy. Specifically, the Peierls stress obtained from the maximum slope of the Peierls barrier differs significantly from that obtained by molecular statics simulations that include the direct application of stress. In order to avoid this drawback, we utilize in the following a recent modification of the NEB method [1] in which only a small number of DOF that represent the position of the dislocation are determined by the NEB force. All remaining DOF are found by constrained molecular statics relaxations while holding the DOF evaluated using the NEB force fixed.

In all the calculations below, the simulated cell is cylindrical. The dislocation line (and thus the z axis) parallel to the $[1\,1\,1]$ direction is placed in the middle of the block along the axis of rotation of the cylinder. In the plane perpendicular to the dislocation glide, the x axis coincides with the $[\bar{1}\,2\,\bar{1}]$ direction, and the y axis with the $[\bar{1}\,0\,1]$ direction. Hence, the xz plane is the $(\bar{1}\,0\,1)$ plane, which is taken as the $\{1\,1\,0\}$ plane most highly stressed by the shear stress driving the dislocation motion. The orientations of the three $\{1\,1\,0\}$ planes in the zone of the $[1\,1\,1]$ slip direction are shown in Fig. 1. In all NEB + r calculations, the elastic band (i.e., the path of the dislocation) is discretized by 15 movable images. The NEB force has only five components and updates only the z coordinates of the five atoms that are closest to the path of the dislocation between two neighboring lattice sites. It was shown in Ref. [1] that the Peierls barriers obtained by the NEB + r method are largely insensitive to the choice of DOF around the dislocation that are updated by the NEB force. The five DOF considered here define the lowest dimensional space for this type of calculation. For example, if the slip plane is the $(\bar{1}\,0\,1)$ plane, i.e., the dislocation moves from site 0 to site A, the atoms associated with the five DOF are marked 1–5 in Fig. 1. The atomic block used in the calculation of the Peierls barrier has to be large enough to make sure that the energies of the initial and final images obtained under the same applied stress are virtually the same. This condition is satisfied if the outer radius of the block is at least $R = 15a$, where a is the lattice parameter (for tungsten, 3.165 Å). In this case, the energy difference between the initial and final configurations at zero applied stress is only 0.002 eV, which is negligible compared with the magnitude of the energy barrier (~0.15 eV). Moreover, the maximum force on any atom allowed in the relaxed initial and final images has to be low enough to guarantee that there are no images of lower energy that could be found by the

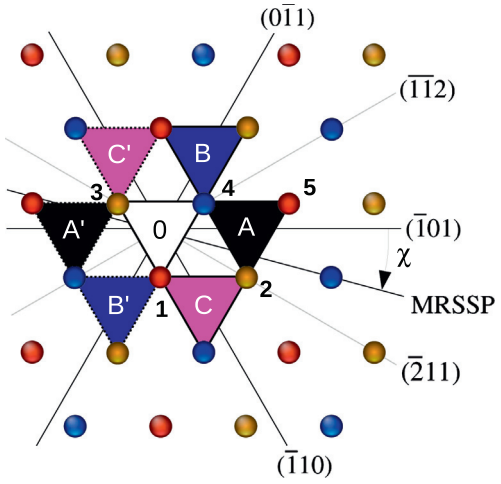

Fig. 1. Geometry of the simulated block showing the orientation of planes and directions used in this paper. The spheres represent positions of atoms in the three successive $(1\,1\,1)$ planes and the initial position of the dislocation corresponds to the lattice site marked "0". Under positive applied shear stress parallel to the slip direction (also in tension), the dislocation can move on the three $\{1\,1\,0\}$ planes in the directions $0 \rightarrow$ A, $0 \rightarrow$ B or $0 \rightarrow$ C. When this shear stress is negative (also in compression), the dislocation moves in directions $0 \rightarrow$ A′, $0 \rightarrow$ B′ or $0 \rightarrow$ C′.

NEB + r calculation at zero applied stress. Here, the molecular statics relaxations are terminated if $\max_i ||\mathbf{F}_i|| < 0.005$ eV/Å, where i passes through all atoms in the block.

When inserting the dislocation or imposing the external stress, all atoms in the block are initially displaced according to the corresponding anisotropic linear elastic strain field [38,39]. The atoms at distances $R < 15a$ from the center of the block are then relaxed, while the atoms outside this region are held fixed. The final configurations of the atomic block that correspond to dislocation positions after its motion along any of the three $\{1\,1\,0\}$ planes of the $[1\,1\,1]$ zone between two neighboring lattice sites are obtained in the same way. The NEB + r method is then applied to calculate the Peierls barriers for the motion of the dislocation along the three possible $\{1\,1\,0\}$ planes. Each of these energy barriers is defined by a discrete set of energies E_I, where $I = \{0, M+1\}$ are the two known fixed images, and $I = 1 \ldots M$ the unknown images in the chain of states of the system (elastic band) that are determined by the NEB calculation. The corresponding energies per unit length of the dislocation are obtained readily as $V_I = E_I / b$, where b is the length of the dislocation segment included in the simulated cell which, in this case, is also the length of the Burgers vector of the dislocation. The Peierls barrier $V(\xi)$ is then obtained by interpolating the discrete set of values $V_I - V_0$ for $I = 0 \ldots M+1$ along the dislocation coordinate ξ. In principle, ξ corresponds to the distance the dislocation moved along a curvilinear path in the $(1\,1\,1)$ plane perpendicular to its line. While it is still an open question whether this dislocation path can be determined uniquely from the knowledge of the positions of atoms, the coordinate ξ is defined as a straight line connecting the two neighboring lattice sites between which the dislocation transits.

This choice is supported by recent calculations in Ref. [33], where an approximate method employing a curved path of the dislocation was introduced. While in calculations using central force potentials of EAM type the path may be significantly curved, the DFT-based calculations, which include implicitly directional bonding just as the bond order potentials do, suggest that this path is not far from being straight.

3. Stress dependence of the Peierls barrier

3.1. Dependence on the shear stress parallel to the slip direction

First, only the shear stress parallel to the slip direction is considered, which is applied in a MRSSP that contains the $[1\,1\,1]$ slip direction. In the right-handed coordinate system, where the y axis is perpendicular to the MRSSP, the z axis parallel to the dislocation line, and the x axis lies in the MRSSP perpendicular to the dislocation line and its Burgers vector, this stress tensor is

$$\mathbf{\Sigma}^{\sigma}_{\mathrm{MRSSP}} = \begin{bmatrix} 0 & 0 & 0 \\ 0 & 0 & \sigma \\ 0 & \sigma & 0 \end{bmatrix}. \tag{2}$$

It is known from molecular statics simulations [2] that the glide plane is $(\bar{1}\,0\,1)$ for any orientation of the MRSSP. If one rotates the coordinate system around the z axis such that the new y axis is perpendicular to the glide plane $(\bar{1}\,0\,1)$ and the x axis is in this glide plane, the stress tensor in this coordinate system is

$$\mathbf{\Sigma}^{\sigma}_{(\bar{1}01)} = \begin{bmatrix} 0 & 0 & \sigma_{13} \\ 0 & 0 & \sigma_{23} \\ \sigma_{13} & \sigma_{23} & 0 \end{bmatrix}. \tag{3}$$

Here, σ_{23} is the shear component of the stress tensor that acts in the $(\bar{1}\,0\,1)$ glide plane parallel to the slip direction and, by definition, it is the Schmid stress driving the dislocation. The shear component σ_{13} is parallel to the slip direction, but acts in the plane perpendicular to the $(\bar{1}\,0\,1)$ plane and does not drive the dislocation. Hence, the latter stress component is called a non-glide stress.

Owing to the additive property of stress tensors, one can express Eq. (3) as a sum $\mathbf{\Sigma}^{\sigma}_{(\bar{1}01)} = \mathbf{\Sigma}^{\sigma}_{\mathrm{nonglide}} + \mathbf{\Sigma}^{\sigma}_{\mathrm{glide}}$, where $\mathbf{\Sigma}^{\sigma}_{\mathrm{nonglide}}$ imposes the non-glide stress (σ_{13}) and $\mathbf{\Sigma}^{\sigma}_{\mathrm{glide}}$ the Schmid stress (σ_{23}). The objective is to investigate how the Peierls barrier for the motion of the dislocation in the $(\bar{1}\,0\,1)$ plane changes with the orientation of the MRSSP. This orientation can be described by the angle χ between the $(\bar{1}\,0\,1)$ plane and the MRSSP (see Fig. 1), which has been commonly used in the literature [2,4,5]. For symmetry reasons, the angle χ can be limited to the range $\langle -30°, 30° \rangle$. By varying the orientation of the MRSSP from negative to positive values of χ, the present authors investigated the well-known twinning–antitwinning asymmetry [4], which should be reflected not only in the Peierls stress, but also in the Peierls barrier. This asymmetry, if observed, results from the non-glide shear stress σ_{13}. While most of the calculations in this paper were made using the BOP for W, the study involving the variation in the orientation of the MRSSP when applying the shear stress parallel to the slip direction was also made for Mo. The reason is that the molecular statics calculations suggest only negligible twinning–antitwinning asymmetry in W when the potential developed in Ref. [35] is used, but a significant one in Mo when the potential developed in Ref. [40] is used.

The following calculations consider the planes $(\bar{3}\,1\,2)$, $(2\,\bar{1}\,3)$ and $(\bar{1}\,0\,1)$ as the MRSSP. The two former planes make angles $\chi = \pm 19.1°$ with the $(\bar{1}\,0\,1)$ plane, which are close to the middle of the angular range of $\pm 30°$; $\sigma_{13} > 0$ for the $(\bar{3}\,1\,2)$ plane, $\sigma_{13} < 0$ for the $(2\,\bar{1}\,3)$ plane and $\sigma_{13} = 0$ for the $(\bar{1}\,0\,1)$ plane. The applied non-glide stress tensor in the coordinate system $x = [\bar{1}\,2\,\bar{1}]$, $y = [\bar{1}\,0\,1]$ and $z = [1\,1\,1]$ is

$$\mathbf{\Sigma}^{\sigma}_{\mathrm{nonglide}} = \begin{bmatrix} 0 & 0 & \sigma_{13} \\ 0 & 0 & 0 \\ \sigma_{13} & 0 & 0 \end{bmatrix}. \tag{4}$$

Starting with the two relaxed atomic blocks in which the dislocation is in two neighboring minimum energy lattice sites in the $(\bar{1}\,0\,1)$ plane, the non-glide stress tensor (4) is then applied by increasing σ_{13} in steps up to the value that it would attain when the stress tensor (2) was applied in molecular statics calculations to the level just before the dislocation started to move, i.e., when $\sigma/C_{44} = \mathrm{CRSS}/C_{44} - 0.001$, where CRSS is the critical resolved shear stress in a given MRSSP. The NEB + r method is then employed to calculate the Peierls barriers in the $(\bar{1}\,0\,1)$ plane when the stress tensor (4) is applied in accordance with the MRSSP considered. These barriers are plotted in the upper panels of Fig. 2a and b for W and Mo, respectively. In all cases studied here and also those calculated in the following sections, the Peierls barriers always possess just one maximum. The same was found in recent studies employing a DFT-based method [31,32], while calculations using central force potentials of EAM type often lead to Peierls barriers with intermediate minima [31,41]. The latter are presumably not physically appropriate for transition metals with mixed directional and nearly free electron bonding.

In the case of W (Fig. 2a), it is observed that when the MRSSP is $(2\,\bar{1}\,3)$ or $(\bar{3}\,1\,2)$ the $(\bar{1}\,0\,1)$ Peierls barrier is lower than for the MRSSP $(\bar{1}\,0\,1)$. Moreover, the barrier is higher for the MRSSP $(\bar{3}\,1\,2)$ than for the MRSSP $(2\,\bar{1}\,3)$, which indicates a twinning–antitwinning asymmetry. The lower panel of Fig. 2a shows the derivatives of the three Peierls barriers. Fig. 2a shows that σ_P is very similar for all three MRSSP, and thus there is almost no twinning–antitwinning asymmetry of σ_P. This agrees with the molecular statics calculations for W [2], where the Peierls stress for the $(\bar{1}\,0\,1)$ plane is equal to $\mathrm{CRSS} \cdot \cos\chi$; this value is practically the same for different MRSSP, as drawn in Fig. 2a by the dashed line. The largest deviation of the Peierls

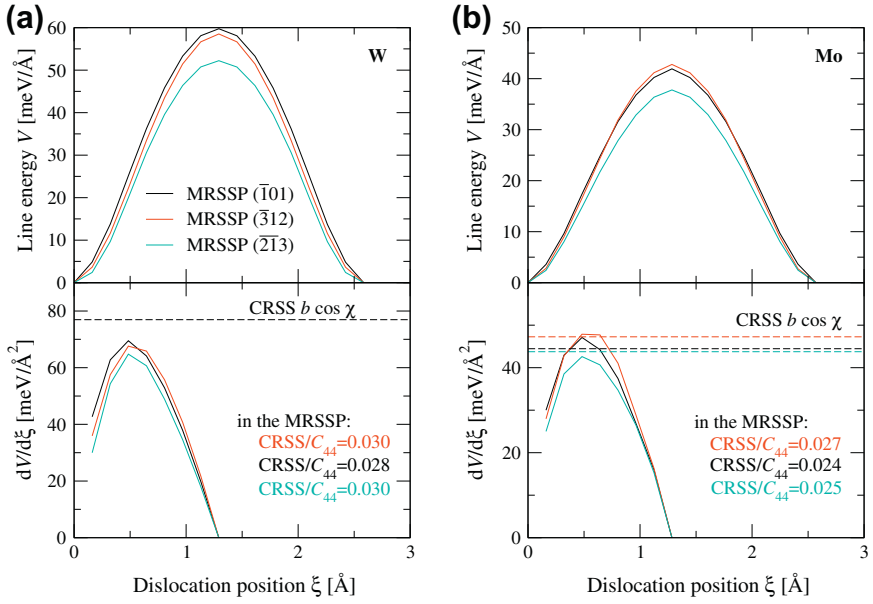

Fig. 2. Variations in the Peierls barriers and their derivatives with the non-glide shear stress σ_{13} (upper panels) for (a) tungsten and (b) molybdenum. The lower panels show the derivatives of these barriers along the dislocation position, defined by the variable ξ. Their maxima determine the corresponding Peierls stresses. Three MRSSP considered are the $(\bar{1}01)$ plane ($\sigma_{13}=0$), $(\bar{3}12)$ for which $\sigma_{13}>0$, and $(\bar{2}\bar{1}3)$ for which $\sigma_{13}<0$. The values of the projection of the CRSS acting in the MRSSP into the $(\bar{1}01)$ plane found in molecular statics calculations (Peierls stresses) are drawn in the lower panels as straight dashed lines.

stress determined from the barriers relative to that calculated by molecular statics is ~15%, which could be further reduced if the exact dislocation pathways were known.

The three Peierls barriers for Mo and their derivatives are shown in the upper and lower panels of Fig. 2b, respectively. Similarly as in the case of W, these indicate a twinning–antitwinning asymmetry that is also clearly visible from the bottom panel of Fig. 2b. Here, σ_P in the $(\bar{1}01)$ plane is the lowest for the MRSSP $(\bar{2}\bar{1}3)$ (twinning sense of shear), intermediate for the MRSSP $(\bar{1}01)$ and highest for the MRSSP $(\bar{3}12)$ (antitwinning sense of shear). The values of σ_P determined from the Peierls barriers agree very well with the Peierls stresses obtained by molecular statics calculations. The latter are depicted in Fig. 2b as dashed lines that are now different for different MRSSP. Small differences between the Peierls stresses calculated from barriers and in molecular statics occur, most likely as a result of the actual curved dislocation path.

Importantly, this calculation demonstrates that the twining–antitwinning asymmetry of the Peierls stress results from the non-glide shear stress σ_{13} that is parallel to the slip direction, but acts in the plane perpendicular to the $(\bar{1}01)$ glide plane. Since the NEB + r method reproduces correctly both the twinning–antitwinning asymmetry in Mo and negligible asymmetry in W, it confirms that this method is a reliable tool for investigating the variation of the Peierls barrier with the non-glide shear stress σ_{13}.

3.2. Effect of shear stress perpendicular to the slip direction

From previous atomistic studies [2,27], it follows that the Peierls stress depends not only on the orientation of the MRSSP, but also on the shear stress perpendicular to the slip direction. For this reason, the changes in the Peierls barrier induced by such shear stress are investigated. This stress is applied by displacing all atoms in the block according to the elastic strain tensor induced by the stress tensor

$$\boldsymbol{\Sigma}^{\tau}_{\mathrm{MRSSP}} = \begin{bmatrix} -\tau & 0 & 0 \\ 0 & \tau & 0 \\ 0 & 0 & 0 \end{bmatrix}, \tag{5}$$

which is applied in the same coordinate system as the stress tensor $\boldsymbol{\Sigma}^{\sigma}_{\mathrm{MRSSP}}$ (Eq. (2)). While there are an infinite number of ways to apply the shear stress perpendicular to the slip direction, the stress given by Eq. (5) was found in earlier studies [2,27] to be the most suitable. It corresponds to a biaxial tension–compression in the plane perpendicular to the dislocation line. Therefore, the plane of the maximum shear stress perpendicular to the slip direction is found by rotating the coordinate system of the tensor (5) by −45° in the [1 1 1] zone.

The initial and final configurations for the NEB + r calculations were obtained by applying $\tau/C_{44} = \{0, \pm 0.02, \pm 0.04\}$ to the block with the dislocation. Since there are three {1 1 0} planes in the [1 1 1] zone, there are 15 possible final configurations for the five initial configurations. The starting and final configurations were obtained by first inserting the dislocation into the closest equivalent lattice sites on $(\bar{1}01)$, $(0\bar{1}1)$ and $(\bar{1}10)$ planes and relaxed by molecular statics at $\tau = 0$. The magnitude of τ was then gradually increased to the desired level, while relaxing the atomic positions using molecular statics at each step.

When the starting and final positions of the dislocation had been defined, the NEB + r procedure was employed to

calculate the 15 energy barriers between the five unique initial atomic configurations and the 15 final configurations that correspond to the motion of the dislocation along the three different {1 1 0} planes. The 15 calculated barriers are shown in the upper row of Fig. 3. If τ increases from zero to positive values, the Peierls barrier for the dislocation motion along $(\bar{1}\,0\,1)$ decreases, while the barriers for the motion on the other two {1 1 0} planes increase. However, when τ decreases from zero to negative values, the Peierls barrier for the dislocation motion on the $(\bar{1}\,0\,1)$ plane increases, while those for the motion on the other two {1 1 0} planes decrease. This variation in the Peierls barrier is reflected in the Peierls stress for the three {1 1 0} planes. This is seen from the bottom part of Fig. 3, where the derivatives of the Peierls barriers are plotted vs. the coordinate ξ. The dislocation moves on the $(\bar{1}\,0\,1)$ plane when $\max(\mathrm{d}V/\mathrm{d}\xi)$ (black curve) agrees with CRSS $\cdot\, b$ (black dashed line). However, the dislocation glides either on the $(0\,\bar{1}\,1)$ or on the $(\bar{1}\,1\,0)$ plane when $\max(\mathrm{d}V/\mathrm{d}\xi)$ (blue or purple curve, respectively) agrees with CRSS $\cdot\, b/2$ (blue dashed line). For $\tau > 0$, $\max(\mathrm{d}V/\mathrm{d}\xi)$, and thus $\sigma_P b$ is always the lowest for the $(\bar{1}\,0\,1)$ plane. Hence, the dislocation is most likely to move on this plane. The magnitude of $\max(\mathrm{d}V/\mathrm{d}\xi)$ agrees well with CRSS $\cdot\, b$ determined by molecular statics. For $\tau < 0$, $\max(\mathrm{d}V/\mathrm{d}\xi)$ is the lowest for the $(\bar{1}\,1\,0)$ plane, which suggests that the dislocation will move on this plane. Indeed, the value of $\max(\mathrm{d}V/\mathrm{d}\xi)$ agrees well with CRSS $\cdot\, b/2$ obtained from molecular statics calculations (blue dashed line), but the slip plane found in molecular statics [2] is $(0\,\bar{1}\,1)$. However, it will be shown in the next section that the Peierls stresses for the $(\bar{1}\,1\,0)$ and $(0\,\bar{1}\,1)$ planes are practically the same when shear stresses both parallel and perpendicular to the slip direction are applied.

At this point, the present authors note that the agreement between the Peierls stress determined from the Peierls barrier and that found in molecular statics calculations is very close for both positive and negative τ, while for $\tau = 0$ the Peierls barrier slightly underestimates the Peierls stress. This suggests that the path of the dislocation in the actual slip plane becomes closer to the assumed straight line as τ deviates from zero. The reason is, presumably, the effect of τ on the core that extends into the $(\bar{1}\,0\,1)$ plane for $\tau > 0$ and into the $(0\,\bar{1}\,1)$ and $(\bar{1}\,1\,0)$ planes for $\tau < 0$. The deviation of the path away from the straight line appears to be the most significant when $\tau \approx 0$.

3.3. Combination of the shear stresses perpendicular and parallel to the slip direction

In the following, a combination of the shear stresses perpendicular (τ) and parallel (σ) to the slip direction is considered, where the latter acts in the MRSSP $(\bar{1}\,0\,1)$ and its magnitude is slightly below the CRSS identified for the given value of τ by molecular statics simulations [2]. Of course, one cannot apply the Peierls stress because the dis-

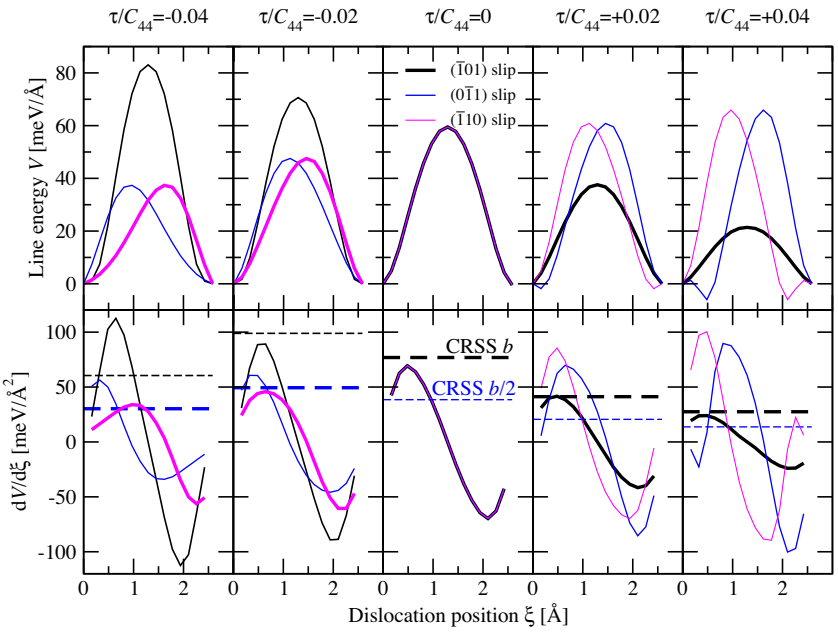

Fig. 3. Variation in the Peierls barrier and the corresponding Peierls stress with the applied shear stress perpendicular to the slip direction (τ) that is applied using the stress tensor (5). For each stress applied, the upper panels show the three Peierls barriers that correspond to elementary steps of the dislocation on $(\bar{1}\,0\,1)$, $(0\,\bar{1}\,1)$ and $(\bar{1}\,1\,0)$ planes; these are drawn in black, blue and purple, respectively. The dislocation moves on the $(\bar{1}\,0\,1)$ plane if CRSS $\cdot\, b$ (black dashed line) coincides with $\max(\mathrm{d}V/\mathrm{d}\xi)$ (black curve). However, it glides on either the $(0\,\bar{1}\,1)$ or $(\bar{1}\,1\,0)$ plane if CRSS $\cdot\, b/2$ (blue dashed line) coincides with $\max(\mathrm{d}V/\mathrm{d}\xi)$ (blue or purple curve, respectively). The curves for predicted slip planes are drawn as thick lines. A small linear correction was applied to the barriers to ensure that the energies of the two fixed images are identical. (For interpretation of the references to color in this figure legend, the reader is referred to the web version of this article.)

location would move, and the initial and final states of the system for the NEB + r calculation could not be identified. Only two shear stresses perpendicular to the slip direction are considered, $\tau/C_{44} = \pm 0.04$. For $\tau/C_{44} = -0.04$, molecular statics calculations give CRSS/$C_{44} = 0.022$ (the slip takes place on the $(0\bar{1}1)$ plane), whereas for $\tau/C_{44} = +0.04$, it is CRSS/$C_{44} = 0.01$ (the slip takes place on the $(\bar{1}01)$ plane).

The initial and final atomic blocks for the NEB + r calculations were obtained by taking the blocks that were relaxed at $\tau/C_{44} = \pm 0.04$ and $\sigma = 0$ and superimposing the shear stress parallel to the slip direction in steps of $0.001\,C_{44}$. The starting configurations of the intermediate images $I = 1 \ldots M$ in the NEB + r procedure were obtained by linear interpolations of the atomic positions from the initial and final states at the given applied stress. In this case, the NEB + r calculations do not provide the Peierls barrier but, instead, the enthalpy of the system per unit length of the dislocation line,

$$H(\xi) = V(\xi) - \sigma b \xi \cos\psi, \tag{6}$$

where $V(0) = 0$ and $\psi = 0$ for the $(\bar{1}01)$ plane, and $\psi = \pm 60^\circ$ for the $(\bar{1}10)$ and $(0\bar{1}1)$ planes, respectively. Here, $\sigma b \xi \cos\psi$ is the work done by the Schmid stress $\sigma\cos\psi$ when moving the dislocation a distance ξ along the dislocation path in the $(\bar{1}01)$, $(0\bar{1}1)$ or $(\bar{1}10)$ planes. It is emphasized that Eq. (6) is not an activation enthalpy that would appear in a mechanism of the thermally activated process of the dislocation motion, since here the movement of a straight infinite dislocation is considered. Instead, it is a measure of the remaining energy that has to be supplied purely mechanically (i.e., by increasing the applied stress σ) to move the dislocation on the slip plane characterized by the angle ψ. The dislocation moves when

$$\max \frac{\mathrm{d}H(\xi)}{\mathrm{d}\xi} \leqslant 0 \tag{7}$$

and it follows from Eq. (6) that

$$\max \frac{\mathrm{d}H(\xi)}{\mathrm{d}\xi} = \max \frac{\mathrm{d}V(\xi)}{\mathrm{d}\xi} - \mathrm{CRSS} \cdot b \cos\psi \tag{8}$$

which uses the fact that CRSS = max σ.

The enthalpies $H(\xi)$ and their derivatives $\mathrm{d}H/\mathrm{d}\xi$ are plotted for the three $\{1\,1\,0\}$ slip planes in Fig. 4. For $\tau/C_{44} = -0.04$, max($\mathrm{d}H/\mathrm{d}\xi$) is very similar for both $(0\bar{1}1)$ and $(\bar{1}10)$ planes, and it is significantly smaller than for the $(\bar{1}01)$ plane. In both cases, max($\mathrm{d}H/\mathrm{d}\xi$) is close to zero and, while inequality (7) is not exactly satisfied; it is likely to be satisfied if the dislocation path deviated from the straight line. Hence, the dislocation can move either on the $(0\bar{1}1)$ or on the $(0\bar{1}1)$ plane, but the preferred slip plane cannot be predicted unambiguously. There is no reason to expect that the distances the dislocation traverses between neighboring minimum energy positions on these two planes, and thus also the corresponding derivatives $\mathrm{d}H/\mathrm{d}\xi$ for these two planes, would be identical. Hence, the corresponding enthalpies $H(\xi)$ may also be different, which would give preference for the slip of the dislocation on one of these $\{1\,1\,0\}$ planes. Repeating this analysis for $\tau/C_{44} = +0.04$ and $\sigma \approx$ CRSS yields the plots shown in the right panels of Fig. 4. Here, the enthalpy for the $(\bar{1}01)$ slip follows inequality (7), while those for $(0\bar{1}1)$ and $(\bar{1}10)$ slips do not. Consequently, there is a clear preference for the slip of the dislocation on the $(\bar{1}01)$ plane as found in the molecular statics calculations [2].

3.4. Uniaxial loading

In the case of uniaxial loading, the applied stress tensor contains not only the shear stresses perpendicular and parallel to the slip direction, but also other stress components such as the hydrostatic stress and the normal stresses perpendicular to the slip direction. However, these stresses cannot influence the Peierls stress unless they are extremely large, in which case they change the nature of bonding. Hence, any uniaxial loading (both tension and compression) can be represented from the point of view of dislocation motion as a combination of the shear stresses perpendicular (τ) and parallel (σ) to the slip direction acting in the MRSSP that are built up simultaneously, such that their ratio ($\eta = \tau/\sigma$) is fixed. For tensile loading ($\tau > 0$), atomistic simulations [2] predict that the dislocation moves on the $(\bar{1}01)$ plane for any orientation of the loading axis. However, in compression ($\tau < 0$), the dislocation may move in a $\{1\,1\,0\}$ plane in which the shear stress parallel to the Burgers vector is lower than in the $\{1\,1\,0\}$ plane with the highest Schmid factor.

As an example of uniaxial loading, the NEB + r calculation of the Peierls barrier for compression in the $[\bar{2}\,3\,8]$

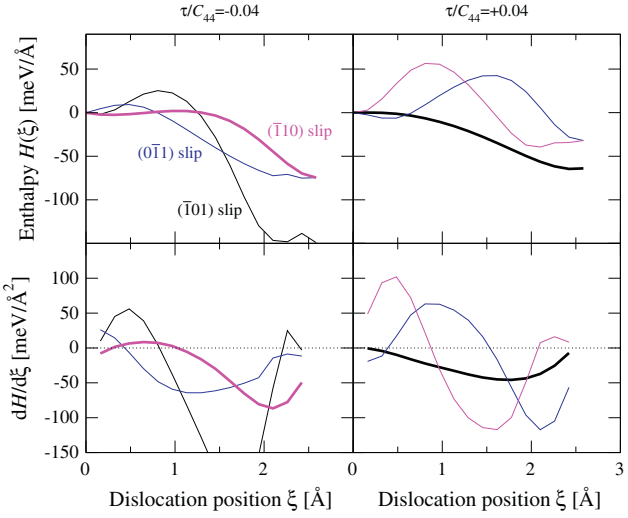

Fig. 4. Enthalpies (upper panels) and their derivatives (lower panels) for the $(\bar{1}01)$ slip (black), the $(0\bar{1}1)$ slip (blue) and the $(\bar{1}10)$ slip (purple), calculated for a combination of the shear stresses perpendicular (τ) and parallel (σ) to the slip direction. The value of σ is slightly below the CRSS for the corresponding value of τ. Left panels: $\tau/C_{44} = -0.04$ and $\sigma/C_{44} = 0.021$; right panels: $\tau/C_{44} = +0.04$ and $\sigma/C_{44} = 0.009$. (For interpretation of the references to color in this figure legend, the reader is referred to the web version of this article.)

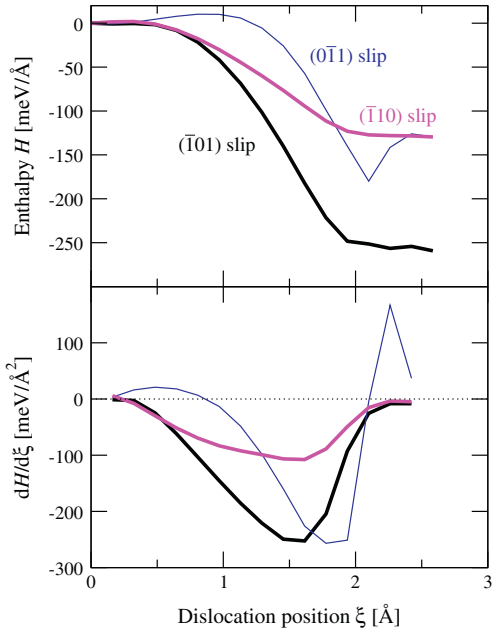

Fig. 5. Enthalpies (upper panel) and their derivatives (lower panel) for the ($\bar{1}$01) slip (black), the (0$\bar{1}$1) slip (blue) and the ($\bar{1}$10) slip (purple) for loading in compression along [$\bar{2}$38]. (For interpretation of the references to color in this figure legend, the reader is referred to the web version of this article.)

direction was carried out, i.e., when the MRSSP is ($\bar{1}$01). As in the previous calculations, the magnitude of the axial stress was chosen such that $|\sigma|$ was slightly below the CRSS obtained by molecular statics calculations for this uniaxial load. In this case, the shear stress parallel to the slip direction is negative, and thus the dislocation moves in the direction opposite to that for the combination of the two shear stresses discussed above. Therefore, the final positions of the dislocation on the three {1 1 0} planes correspond to the points marked A′, B′, C′ in Fig. 1.

The calculated enthalpies for the motion of the dislocation along the three {1 1 0} planes are shown in the upper panel and their derivatives in the lower panel of Fig. 5. One can see that $\max(dH/d\xi) \approx 0$ for both ($\bar{1}$01) and ($\bar{1}$10) planes. Hence, the dislocation is equally likely to glide on these two {1 1 0} planes. This agrees with the results of the application of stress in molecular statics calculations, where the dislocation was found to move on the ($\bar{1}$10) plane for the [$\bar{2}$38] compression, but a small deviation in the loading axis towards the [0 1 2] direction causes a change of the slip plane to the ($\bar{1}$01) plane [42].

4. Comparison of the Peierls barriers determined by NEB calculations with those constructed based on Peierls stresses calculated by molecular statics

The previous sections presented calculations of the Peierls barriers using the modified NEB + r method for several special orientations of loading, and demonstrated that the Peierls stresses deduced from these barriers agree closely with those evaluated in molecular statics calculations. As stated already in the Introduction, the reason for determining the Peierls barrier and its stress dependence is that this is a precursor for the development of a mesoscopic theory of thermally activated dislocation motion for any loading of a single crystal. However, for this purpose, the Peierls barriers would have to be evaluated for a broad variety of externally applied loads, and this is computationally very demanding when employing the NEB method. In a previous study [3], the present authors proposed an approximate but computationally much less demanding approach for estimating the Peierls barrier and its dependence on external loading directly from the corresponding dependence of the Peierls stress found in molecular statics calculations. This section compares this approach with the NEB + r calculations and assesses in this way its applicability and limitations.

In Ref. [3], the present authors first introduced the Peierls potential in a generic two-dimensional form as a mapping function that reflects the threefold symmetry of the [1 1 1] axis and the positions of potential minima and maxima. This mapping function was not obtained by any calculations, and its sole purpose was to serve as a template that reflects the symmetry of the lattice. The loading by shear stresses parallel and/or perpendicular to the Burgers vector deforms the Peierls potential so that it becomes asymmetric. Starting with the generic symmetric form of the Peierls potential, its asymmetry arising from applied shear stresses was determined such as to reproduce the variations of the Peierls stress with the orientation of the MRSSP and with the shear stress perpendicular to the slip direction, as obtained in molecular statics calculations. The details of the parameterization of the Peierls potential and calculation of the related Peierls barriers for a given loading are found in Ref. [3].

As an example, Fig. 6 shows a comparison between the Peierls barriers calculated by the NEB + r method and those obtained in Ref. [3] for the case of loading by a shear stress τ perpendicular to the Burgers vector. In the former case, the dislocation is assumed to move along a straight line connecting the two neighboring lattice sites in the slip plane, while in the latter case the path may not coincide with the straight line. Both calculations predict that, for $\tau \geqslant 0$, the glide of the dislocation takes place on the ($\bar{1}$01) plane, while for $\tau < 0$ the slip plane is ($\bar{1}$10). The maximum slopes of the Peierls barriers for the slip planes are quite similar and very close to the product CRSS $\cdot\, b$ when the glide plane is ($\bar{1}$01) and to CRSS $\cdot\, b/2$ when the glide plane is ($\bar{1}$10). However, the overall shapes of the barriers calculated in the two different ways are significantly different, in particular close to their maxima. This is understandable, since only the maximum slope of the Peierls barrier calculated by the approach used in Ref. [3] is fitted to the Peierls stress obtained by molecular statics, but no information about the barrier height and shape enters this procedure. Nevertheless, the method developed in Ref. [3], which is computationally much less demanding, can be

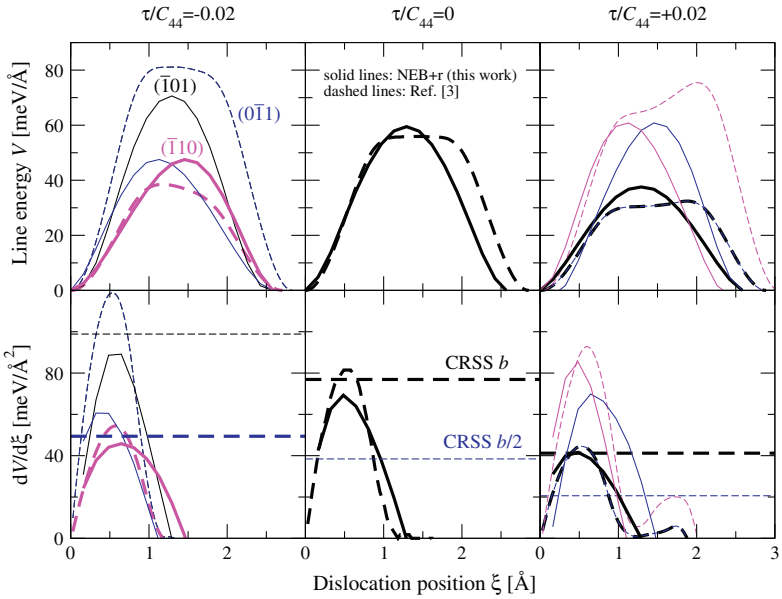

Fig. 6. Comparison of dependencies of the Peierls barriers and their derivatives on the shear stress perpendicular to the slip direction obtained in the present study and in Ref. [2] for the three $\{1\,1\,0\}$ planes. The solid curves correspond to the barriers calculated by the NEB + r method (this work), and the dashed curves are determined from the generic two-dimensional Peierls potential parameterized such as to reproduce molecular statics calculations of the Peierls stress in Ref. [2]. The thick curves represent the Peierls barriers for the actual glide plane, i.e., $(\bar{1}\,0\,1)$ for $\tau \geqslant 0$ and $(\bar{1}\,1\,0)$ at $\tau < 0$. The blue and black dashed curves coincide, which is a consequence of the way the asymmetry of the Peierls potential is incorporated into the model developed in Ref. [2]. (For interpretation of the references to color in this figure legend, the reader is referred to the web version of this article.)

used, but the height and shape of the barrier near the maximum need to be modified. This can be done by comparison with a few representative calculations of the Peierls barrier employing the approach discussed in this paper or, when developing the model of the thermally activated motion of dislocations, by additional fitting of the flow stress at a chosen temperature and loading to experimental values. The latter was used in Ref. [3].

5. Conclusions

The main result of this paper is the dependence of the Peierls barrier of $1/2\langle 1\,1\,1\rangle$ screw dislocations in bcc metals on the applied stress tensor. This investigation was carried out by employing the recently formulated NEB method with constrained atomic relaxations (NEB + r) [1] and describing the interaction between the atoms using a bond order potential for tungsten [35]. However, the general results are not sensitively dependent on the potential used and can be considered as common for all transition bcc metals. Since no reliable procedure exists that would determine the possible curved shape of the dislocation path, the usual assumption was adopted that the dislocation moves along a straight line connecting the neighboring minimum energy dislocation positions. This choice is supported by the recent calculations employing a DFT-based method [31,33]. As suggested by molecular statics calculations [2], the motion of an isolated $1/2[1\,1\,1]$ screw dislocation always occurs along one of the three $\{1\,1\,0\}$ planes of the $[1\,1\,1]$ zone. Following the dependence of the Peierls stress on the form of the applied stress found in these calculations, the present authors deem that the Peierls barrier depends on the following non-glide shear stresses: (i) shear stress parallel to the slip direction, but acting in the plane perpendicular to the slip plane, and (ii) shear stress perpendicular to the slip direction. The former is responsible for the twinning–antitwinning asymmetry of the CRSS, which has been much studied in the literature.

When imposing the shear stress parallel to the slip direction in the plane perpendicular to the slip plane, the effect on the Peierls barrier was very small in the case of W. This means that the twinning–antitwinning asymmetry in W is negligible when the potential from Ref. [35] is used. This agrees with the results of previous molecular statics calculations [2]. However, a test calculation for molybdenum, in which a significant twinning–antitwinning asymmetry was found [2], revealed a significant influence of the shear stress parallel to the slip direction acting in the plane perpendicular to the slip plane.

However, a very significant dependence of the Peierls barrier on the shear stress perpendicular to the slip direction (τ) was always found, as similarly observed in molecular statics calculations [2]. In particular, for $\tau > 0$, the Peierls barrier is the lowest for the motion of the dislocation along the $(\bar{1}\,0\,1)$ plane that coincides with the MRSSP. However, the Peierls barrier for the $(\bar{1}\,1\,0)$ slip is the lowest at negative τ, even though the MRSSP is still the $(\bar{1}\,0\,1)$ plane. The former is fully consistent with the molecular statics calculations [2], where the dislocation always moves on the MRSSP $(\bar{1}\,0\,1)$ under positive τ. However, for negative τ, the molecular statics calculations [2] predict the slip on the $(0\,\bar{1}\,1)$ plane that seemingly contradicts the prefer-

ence for the $(\bar{1}10)$ slip obtained from NEB + r calculations. Nevertheless, it has been shown here that if shear stresses both perpendicular and parallel to the slip direction are applied, as they are in the molecular statics calculations, the maximum derivative of the enthalpy of the system vanishes virtually simultaneously for both moves along $(0\bar{1}1)$ and $(\bar{1}10)$ planes. Hence, any of these planes can become the slip plane at negative τ. This finding agrees not only with the atomistic simulations on bcc tungsten, but also with bcc molybdenum, where at intermediate negative τ the dislocation first glides on the $(0\bar{1}1)$ plane and for large negative τ it cross-slips into the $(\bar{1}10)$ plane [2].

It was also demonstrated here that the NEB + r method predicts the correct Peierls barrier for uniaxial loading. In particular, it was shown that the slip plane under compression in the $[\bar{2}38]$ direction can be either $(\bar{1}01)$ or $(\bar{1}10)$. This agrees with direct atomistic calculations [42] that predict the slip on $(\bar{1}10)$, while a small deviation in the loading direction towards the [012] axis (corresponding to the same MRSSP) changes the slip plane to $(\bar{1}01)$.

The Peierls barriers obtained in this paper using the NEB + r method were compared with those from a much simplified formulation of the Peierls potential that was developed in Ref. [3]. The maximum slopes of both these barriers are essentially the same, but the barriers are quite different close to their maxima. This difference is largely a consequence of a generic shape of the Peierls potential assumed in Ref. [3], which was subsequently parameterized to reproduce the curvature of the stress dependence of the activation enthalpy at intermediate stresses. Since the shape of the Peierls barrier was not known, an infinite number of different barriers could be defined, all of which agree with molecular statics simulations. The NEB + r calculations in this paper remove this ambiguity by providing the shape of the Peierls barrier and its changes under stress without any a priori assumptions about their shapes. This opens the possibility of formulating a novel description of the thermodynamics of dislocation glide that incorporates a correct shape of the Peierls barrier and its changes under stress, as obtained from the NEB + r calculations.

Acknowledgements

RG acknowledges support from the Czech Science Foundation, Grant No. P204/10/0255, from the Marie-Curie International Reintegration Grant No. 247705 "MesoPhysDef", and partial support from the Academy of Sciences of the Czech Republic, Project No. RVO:68081723. VV was supported by the US Department of Energy, Office of Basic Energy Science, Grant No. DE-PG02-98ER45702. The access to the MetaCentrum computing facilities provided under the program "Projects of Large Infrastructure for Research, Development, and Innovations" LM2010005 funded by the Ministry of Education, Youth, and Sports of the Czech Republic is appreciated. This work has been carried out at the Central European Institute of Technology (CEITEC) with research infrastructure supported by project CZ.1.05/1.1.00/02.0068 financed from the EU Structural Funds.

References

[1] Gröger R, Vitek V. Model Simul Mater Sci Eng 2012;20:035019.
[2] Gröger R, Bailey AG, Vitek V. Acta Mater 2008;56:5401.
[3] Gröger R, Vitek V. Acta Mater 2008;56:5426.
[4] Christian JW. Metall Trans A 1983;14:1237.
[5] Duesbery MS. In: Nabarro FRN, editor. Dislocations in solids, vol. 8. Amsterdam: Elsevier; 1989. p. 67.
[6] Taylor G. Prog Mater Sci 1992;36:29.
[7] Seeger A. J Phys IV 1995;5:45.
[8] Pichl W. Phys Stat Sol (a) 2002;189:5.
[9] Vitek V, Paidar V. In: Hirth JP, editor. Dislocations in solids, vol. 14. Amsterdam: Elsevier; 2008. p. 439.
[10] Kocks UF, Argon AS, Ashby MF. Prog Mater Sci 1975;19:1.
[11] Suzuki T, Takeuchi S, Yoshinaga H. Dislocation dynamics and plasticity. Berlin: Springer; 1985.
[12] Cottrell AH. Philos Mag Lett 2002;82:65.
[13] Caillard D, Martin JL. Thermally activated mechanisms in crystal plasticity. Oxford: Pergamon Press; 2003.
[14] Marian J, Cai W, Bulatov VV. Nat Mater 2004;3:158.
[15] Chaussidon J, Fivel M, Rodney D. Acta Mater 2006;54:3407.
[16] Rodney D. Phys Rev B 2007;76:144108.
[17] Rodney D, Proville L. Phys Rev B 2009;79:094108.
[18] Eshelby JD. Proc Roy Soc Lond 1962;266:222.
[19] Brailsford AD. J Appl Phys 1970;41:4439.
[20] Mason WP, MacDonald DE. J Appl Phys 1971;42:1836.
[21] Smith RF, Eggert JH, Rudd RE, Swift DC, Bolme CA, Collins GW. J Appl Phys 2011;110:123515.
[22] Dorn JE, Rajnak S. Trans AIME 1964;230:1052.
[23] Guyot P, Dorn JE. Can J Phys 1967;45:983.
[24] Lau SS, Dorn JE. Phys Stat Sol (a) 1970;2:825.
[25] Liu GC, Lau SS, Dorn JE. Phys Stat Sol (a) 1972;11:645.
[26] Duesbery MS, Vitek V. Acta Mater 1998;46:1481.
[27] Ito K, Vitek V. Philos Mag A 2001;81:1387.
[28] Vitek V, Mrovec A, Gröger R, Bassani JL, Racherla V, Yin L. Mater Sci Eng A 2004;387–389:138.
[29] Henkelman G, Johannesson G, Jónsson H. In: Schwartz SD, editor. Progress on theoretical chemistry and physics. Dordrecht: Kluwer; 2000. p. 269.
[30] Jónsson H, Mills G, Jacobsen KW. In: Berne BJ, Ciccotti G, Coker DF, editors. Classical and quantum dynamics in condensed phase simulations. Singapore: World Scientific; 1998. p. 385.
[31] Proville L, Ventelon L, Rodney D. Phys Rev B 2013;87:144106.
[32] Ventelon L, Willaime F. J Comput-Aid Mater Des 2007;14:85.
[33] Ventelon L, Willaime F, Clouet E, Rodney D. Acta Mater 2013;61:3973.
[34] Pizzagalli L, Beauchamp P, Jónsson H. Philos Mag 2008:88.
[35] Mrovec M, Gröger R, Bailey AG, Nguyen-Manh D, Elsässer C, Vitek V. Phys Rev B 2007;75:104119.
[36] Henkelman G, Jónsson H. J Chem Phys 2000;113:9978.
[37] Henkelman G, Uberuaga BP, Jónsson H. J Chem Phys 2000;113:9901.
[38] Eshelby JD, Read WT, Shockley W. Acta Metall 1953;1:251.
[39] Hirth JP, Lothe J. Theory of dislocations. Chichester: J. Wiley; 1982.
[40] Mrovec M, Nguyen-Manh D, Pettifor DG, Vitek V. Phys Rev B 2004;69:094115.
[41] Gordon PA, Neeraj T, Mendelev MI. Philos Mag 2011;91:3931.
[42] Gröger R. Ph.D. Thesis, University of Pennsylvania; 2007.